ELSEVIER

Human Movement Science 19 (2000) 597–626

HUMAN MOVEMENT SCIENCE

www.elsevier.com/locate/humov

Repeatable spatial maps of a few force and joint torque patterns elicited by microstimulation applied throughout the lumbar spinal cord of the spinal frog

S.F. Giszter [a,*], E. Loeb [b], F.A. Mussa-Ivaldi [c], E. Bizzi [d]

[a] *Department of Neurobiology and Anatomy, Medical College of Pennsylvania/Hahnemann Medical School, Allegheny University of the Health Sciences, 3200 Henry Ave., Philadelphia, PA 19129, USA*

[b] *Netcapitol Inc., Washington, DC, USA*

[c] *Department of Physiology and Department of Physical Medicine and Rehabilitation, Northwestern University Medical School, Chicago, IL, USA*

[d] *Department of Brain and Cognitive Science, MIT, Cambridge, MA, USA*

Abstract

Motor learning and construction of novel behavior must be constrained by the spinal motor apparatus and how it supports movement. Recent work supports a modularity of spinal cord function in both mammals and lower vertebrates. We sought to extend these analyses by a complete mapping of the lumbar enlargement not previously attempted. The frog lumbar spinal cord grey matter motor responses were systematically mapped using microstimulation at a fine grain of 200 μm separation mediolaterally and in depth throughout the enlargement. The patterns of force magnitude and direction were noted. Large areas of spinal cord produced very small forces. Some areas produced strong responses. Both the strong and the weak force responses fell into a few classes. In all frogs examined the forces elicited fell into a few (5) classes of directions. These forces were expressed as joint torques by standard means. Forces were observed to comprise both pure hip torques and combined knee/hip torque patterns, but no pure knee torques. The contiguous regions producing these force directions at high magnitudes were arranged in repeating patterns. The directions of the forces elicited were strongly

* Corresponding author. Tel.: +1-215-991-8412; fax: +1-215-843-9082.
E-mail address: simon@swampthing.neurobio.mcphu.edu (S.F. Giszter).

0167-9457/00/$ - see front matter
PII: S0167-9457(00)00029-4

correlated among frogs in specific regions of spinal cord while other regions showed individual variations. The data are consistent with microstimulation recruitment of specific motor responses or force-field primitives in some spinal cord regions in the frog. Similar constraints may exist early in mammalian motor development or after spinal cord injury.

Keywords: Spinal organization; Motor primitives; Force fields; Reflex control; Limb mechanical properties

1. Introduction

Previous results obtained from microstimulation of frog spinal cords showed that activation of intermediate areas of spinal cord grey matter produced a few patterns of forces (Bizzi, Mussa-Ivaldi & Giszter, 1991; Giszter, Mussa-Ivaldi & Bizzi, 1993; Loeb, Giszter, Borghesani & Bizzi, 1993; Mussa-Ivaldi & Bizzi, 1994). This observation suggested that there may exist a few primitives or modules in the spinal cord that are used for controlling force and movement in reflex and perhaps in voluntary movements. The attractive features of this idea are several fold. First, the use of functional or anatomical modules to coalesce joint and muscular degrees of freedom into useful assemblies directly addresses Bernstein's formulation of the degrees of freedom problem (Bernstein (1967) and Windhorst (1991); Nichols (1994) and Loeb (2000) for an alternate view). Second, the possibility of the assembly of these modules, primitives or building blocks into new behaviors provides the CNS a means to simply develop new tasks (Mussa-Ivaldi, 1992; Mussa-Ivaldi & Giszter, 1992; Mussa-Ivaldi, 1997). Developmentally the intrinsic primitives may 'bootstrap' novel motor learning. The advantage of primitives is that learning begins from a collection of developmentally and evolutionarily selected assemblies of proven efficacy which will seed motor searches in useful areas of the high dimensional search space in a way not possible in tabula rasa mechanisms (Gandolfo, Mussa-Ivaldi & Bizzi, 1996; Zaal, Daigle, Gottlieb & Thelen, 1999). Third, modular organizations may provide stability guarantees that constrain motor search to safe regions of actuation space and control (Cannon & Slotine, 1995; Lohmiller & Slotine, 1998). Fourth, current control ideas are very clear on the need for modularity, encapsulation and stability of component subunits, modules, primitives, agents or holons in flexible reconfigurable many degrees of freedom processes (Mataric, Williamson, Demiris & Molan, 1998; Kiehn, Hounsgard & Sillar, 1997). If an

organizational principle is useful, it seems to us it is likely that biological evolution will have discovered it or something superior.

Moving beyond microstimulation, extensive examination of reflex behaviors has shown that the analysis of these as collections of flexibly assembled primitives may offer insights and parsimonious accounts of trajectory construction and control (Kargo & Giszter, 2000a,b; Giszter & Kargo, 2000; Tresch, Saltiel & Bizzi, 1999). However, the detailed analysis of microstimulation responses of spinal cord may give insight into whether anatomical modularity supports the functional modularity that is becoming established. This direction is also medically important, since intraspinal FES may soon be developed and effective dynamical controls will be critical (Giszter, Grill, Lemay, Mushahwar & Prochazka, 2000).

The previous studies using microstimulation concentrated on the spatial organization of isometric forces throughout the limb's workspace and the rules of combination for these force-fields when elicited by multiple stimulation. Fields were generally convergent and were found to be scaled in magnitude with increasing stimulation strength or duration. Further, these force-field types could usually ($\sim$80% of trials) be combined by simple vector superposition. More recently Kargo and Giszter (2000a) showed online adjustments of aimed reflex trajectories could be expressed as force-field primitive sums.

Early work suggested that these primitives might be located in specific regions in the spinal cord (Bizzi et al., 1991). More recent testing using microiontophoresis of NMDA also showed similar results (Saltiel, Tresch & Bizzi, 1998).These earlier maps rested on fairly sparse random samples of strong force field responses combined across several frogs. Moreover, depth of the stimulating electrode and the variations in the thresholds and sensitivity to electrical stimulation were largely neglected in the first microstimulation studies. Systematic detailed maps of individual frogs, and their comparisons have not been presented.

The goal of the present study was to validate and extend the earlier work by using a systematic measurement grid at a fine grain in individual frogs and comparing among these. The data to be described here examine the spatial variations of force production and muscle activity across the entire lumbar spinal cord in six frogs. Different regions of spinal cord are likely to have differing processing roles and inputs. We used the maximum spatial resolution compatible with excluding the activation of similar neuron cell bodies at different electrode locations using the chosen stimulation parameters. We summarized our data as three dimensional maps of the lumbar cord. In order

to generate these maps we focussed on measurement of force samples at a fixed limb configuration. We chose a configuration at which the several two dimensional force-fields characterized in earlier work could be distinguished using a single measurement. The force vectors measured at this point in each of the different force fields identified previously differed from one another by more than 10° in orientation. Thus a single measurement indicated which field of the set was represented at that location, but plainly did not fully characterize the field structure. This restriction of data collection to single force vectors rather than complete fields was necessary to make the extensive mapping experiments feasible. Full force-field collection at the density of sampling and current variations used here would not have been possible due to the data explosion of at least an order of magnitude which is required for two dimensional field description. This paper expands on the prior results, by examining three-dimensional forces rather than two-dimensional, including a detailed study of three-dimensional structure of anatomical regions of strong force production due to stimulation within spinal cord and comparing the repeatability and similarity of the elicited cord responses among frogs.

The data collected here show that only a few force directions are represented in the microstimulation data at the limb configuration chosen throughout the entire spinal cord. The areas of high force production are quite localized. Further, the data also demonstrate that the spinal cord spatial distributions of force directions elicited by microstimulation are, as has been assumed in our other work, similar among frogs in many regions of spinal cord and can be related to the segmental and dorso-ventral structure of spinal cord. These suggest that some anatomical modularity may be present, and support novel medical devices which are indwelling in the isolated spinal cord of para or tetraplegic patients (Giszter et al., 2000; Mushahwar, 1996; Lemay & Grill, 1999).

2. Methods

Frogs were transected at the calamus scriptorius, the rostral fore and midbrain structures were destroyed, and the lumbar spinal cord was exposed as described in Giszter et al. (1993). Eleven muscles were implanted with pairs of electromyogram (EMG) electrodes. The frogs were clamped at the pelvis and along the vertebral processes. The pelvis and spinal column thus formed a solid ground base for force production, and allowed stable microstimulation of the exposed spinal cord. Using an ATI 3/10 six axis force sensor mounted

on a cartesian manipulator, the limb was clamped just above the ankle. Thus four proximal degrees of freedom were available. We proceeded to measure all sensor forces and torques and the limb was positioned at a standard configuration (Fig. 1). Link lengths were typically about 5.5 cm for the thigh and 5.0 cm for the shank with the sensor attachment reducing apparent shank length by about 0.5 cm. This configuration corresponded to approximate hip azimuth of 15° rotated towards caudal measured from the mediolateral axis and knee flexion internal angle of 80°. At this posture the limb end-point was located in a region where the four force-fields described in previous work (Bizzi et al., 1991; Giszter et al., 1993) could be distinguished by a single measurement of the two degree of freedom horizontal plane 'active force'. We measured the full six degree of freedom force and torque pattern at the ankle using the sensor. As in previous work (Giszter et al., 1993) 'resting' forces and torques were removed from the measurement by subtraction of pre-stimulus resting measurements. The resultant provides what we have termed 'active' forces represented muscle generated forces above basal tonus and the passive elastic properties of soft tissues, ligaments and resting muscle. To a first approximation, the frog limb in the apparatus when help clamped at the ankle is a four degree of freedom linkage (three rotation axes at the hip and one at the knee). The six degree of freedom measurements using the ATI sensor were thus constrained to a four degree of freedom manifold. Using ankle translational forces as three degrees of freedom to represent this manifold a fourth degree of freedom remained. This was represented by torque production about the axis from the ankle to the acetabulum (the polar direction of the ankle is the hip/ankle axis). We confirmed that our sensor always measured a torque about this hip directed axis in different locations as a control. In this paper however we restrict examination to the three-dimensional translational forces. The torque driving the limb to rotate out of the plane in which it was clamped was small although not negligible. In previous gimbaled measurements (Mussa-Ivaldi et al., 1994) static translational forces were generally little affected by such rotations (and see Mussa-Ivaldi & Gandolfo, 1993). It is important to note that, following the initial placement, the limb was never again moved during the course of these experiments. This is in contrast to previous studies in which forces were sampled at many different locations in order to construct force-fields. A single stainless steel fine microelectrode (Frederick Haer, 10–12 Mohm impedances, $\sim$1 μm tips) was positioned on the pia at 200, 400 or 600 μm from the midline and advanced down into the spinal cord in 200 μm increments. At each site at which the electrode was paused stimulations were

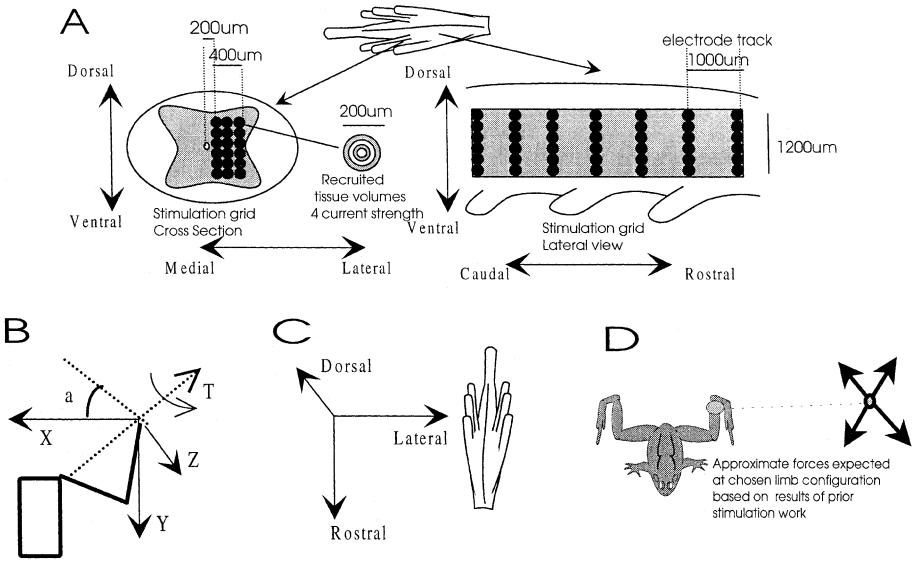

applied (1–8 μA, 0.5 ms pulses, in 40 Hz trains of 300 ms duration) and force and EMG measurements made. Current density and charge passage were estimated to be unlikely to cause tissue damage over time, based on published data (e.g. Grill & Wang, 1997; Mushahwar, 1996; Mushahwar & Horch, 1997). These sets of measurements were repeated at 1 mm intervals rostrally and caudally throughout the extent of the lumbar cord. At each spinal cord site the neural tissues were stimulated through the electrode with cathodal stimuli of 1, 2, 4 and 8 μA using a BAK BSI/2 constant current isolator. Data were collected over a 1 s period for each stimulus. Forces were collected at 85 Hz from the ATI 3/10 and electromyogram activities (EMG) from each of the 11 muscles were collected at 1000 Hz. To confirm electrode stability and response repeatability we occasionally returned to cord sites during mapping. There was little alteration in spinal cord response over several hours, and between different days. Mapping usually took about 8 h sometimes separated into two 4 h sessions on consecutive days. On the second day test locations were compared from the first to ensure stability of the spinal cord state. After the mapping was completed, marking lesions were placed in the cord using 10 μA anodal current for 15 s. These lesions confirmed electrode spacing and relation to cord structure. Iron deposition at lesion sites was revealed using prussian blue counterstained with cressyl violet. The lesions demonstrated that the region of sampling spanned the entire spinal grey from upper surface

Fig. 1. (A) The locations of stimulation in the cord. Stimulation was applied at site separate by 200 μm mediolaterally and in depth (left in cross section of spinal cord). The rostrocaudal interval was generally 1000 μm though some maps were collected at 500 μm rostrocaudal intervals (right in lateral view). The volumes of activated tissue expected from current activation of cells can be represented as spheres which almost touch tangentially at the highest stimulation strength of 8 μA and increase linearly in radius over the four stimulation strengths (1, 2, 4, 8 μA). These are shown in a spinal cord cross section and in a lateral view (parasagittal section). (B) schematic of geometry of frog and limb in relation to force sensor and axes used in subsequent figures (see also panel 1D). The rectangle represents the firmly clamped pelvis, the frog's snout is towards the bottom of the page. The hind-limb represents a 2 link four degree of freedom linkage (bold) from the hip to the interaction port at the attached force sensor. The isometric proximal force production can be represented as four joint torques, or three translational forces and a torque at the measurement point (see Asada & Slotine, 1986). The latter representation is used in this study except where noted. The forces and torques measured at the ankle are referenced to the body as shown here. This panel matches C. Thus *X* axis force is in the cartesian lateral to medial (LM) direction in relation to the body and the spinal cord coordinate system used in mapping, *Y* axis force is in the caudo rostral (CR) direction. The two *X* and *Y* force components represent the planar forces (as e.g. in Kargo & Giszter, 2000a and in Giszter et al., 1993) and lie in the plane of the hind-limb. In the illustration they are in the plane of the paper. *Z* force arises from these as defined by a right handed coordinate system (dorsal ventral (DV) in relation to the frog and spinal cord system in C. The *Z* force drops perpendicularly from the plane of the figure but is drawn in a semi-perspective view. In addition to interaction port forces that are balanced by hip azimuth torque, knee torque and hip elevator torque, the frog generates torque about the polar direction connecting ankle and hip (shown as T). Angular coordinates for the frog are also described here. Hip azimuth angle for the left leg is measured in a clockwise direction about *Z* referenced to the mediolateral or *X* axis. (C) The coordinate system in which spinal cord maps are drawn in relation to the body and force axes shown in b. In effect the force coordinate system is rotated 180° about the rostrocaudal axis so *Z* is pointing in the ventral direction. Thus Rostral axis (caudal to rostral, CR) in map coordinates is also direction of positive *Y* forces, while lateral direction (medial to lateral, ML) in maps is the direction of negative *X* forces and Dorsal direction (ventral to dorsal, VD) in maps is the direction of negative *Z* force. The axes in Figs. 2–9 then can be directly related to B and C. (D) The approximate relationship of the limb ankle location, sensor and the previous force data. The limb configuration was 15° caudal (anticlockwise) to the *X* or mediolateral axis (shown in B and C) axis at the hip and 80° internal angle at the knee. At the ankle location at which forces were collected we expected that the force-fields observed in previous work would produce four distinguishable and different force vectors in the horizontal plane (indicated to the right). The limb location was thus at a site in the force field that should distinguish the four force-field types. In addition, in this study the vertical force component was considered.

of the grey down to the region of motor nuclei and had an error of alignment of under 100 μm mediolaterally and of under 300 μm in depth.

2.1. Data processing

1 kHz EMG data were rectified, smoothed with a 30 point tapered moving average filter, and integrated over 10 ms bins. The peak EMG, the total area of the rectified EMG envelope, and the time of peak EMG were calculated. The peak force and time of occurrence of peak force were measured. EMG

were examined as functions of spatial position in the cord using Explorer software, and inner product correlations.

2.2. Spatial interpolation

The collection of forces and EMG samples formed a regular grid throughout the lumbar cord. We used the Delaunay triangulation algorithm (see Preparata & Shamos, 1988) to construct a collection of non-overlapping tetrahedra which spanned the convex hull of the test data. A sample data point was located at each vertex of each of the tetrahedra comprising the tesselation. We used piecewise linear interpolation within each such tetrahedron to estimate the force and EMG values between sample locations. Data were then further analyzed on an IBM PC using in-house programs, a Sun Sparcstation using custom programs in the S-plus 3.0 language or a Silicon Graphics Indigo 2 workstation using the Explorer data visualization package and in-house software. Isovalue surfaces were constructed in Explorer to display spinal cord volumes with particular response properties. These surfaces were constructed by the Explorer software using the marching cubes algorithm (Lorenson & Cline, 1987). Density and grain of the interpolation of the data which were passed to the Explorer program were varied to confirm that the presence of the structures seen in isosurfaces was not an artifact of the algorithms used in these calculations.

2.3. Three-dimensional polar distributions and smoothing

The complete sets of data from each cord that were collected at a given stimulation strength were assessed as a population of samples from that spinal cord (i.e. irrespective of location of origin within spinal cord). These data were plotted as collections of vectors. Each frog's population of vectors had been sampled so as to have a uniform spatial distribution of samples. In contrast the force directions and amplitudes and EMG responses of each population demonstrated non-uniform distributions. To examine the distribution of force directions, EMG magnitude and force magnitude we constructed distributions of these parameters after directional filtering with a simple smoothing kernel. At uniform angular intervals of azimuth and elevation over the unit sphere the kernel was used to estimate the average magnitude at that particular direction by a summation and averaging of all sample vectors that lay within the circular cone of internal angle q. The selected sample vectors (say n vectors: $\mathbf{v}_1 \ldots \mathbf{v}_n$) inner products with the unit

direction vector of the principal axis of the cone were summed, and then divided by the number of sample vectors lying within the cone of angle q, i.e.,

$$\boldsymbol{V} \equiv k \cdot \boldsymbol{V_d} \cdot \frac{\sum_{i=1}^{i=n} [\boldsymbol{v_i} \cdot \boldsymbol{v_d}]}{n} \tag{1}$$

for direction $\boldsymbol{V}_d$.

k is a global weighting constant based on the cone angle q which may be chosen to preserve the magnitude of the integral of the total distribution or for graphical scaling and n is the number of samples falling within the cone. In general cones of $q = 0.3$–0.5 radians were used in smoothing.

In this way we constructed smooth three dimensional surfaces representing the relationship of mean force magnitude to direction.

Similarly, the shape of the probability density for all force directions was estimated using

$$\boldsymbol{V} = \boldsymbol{V}_d \cdot k \cdot \frac{\sum_{i=1}^{i=n} \frac{[\boldsymbol{v}_i \cdot \boldsymbol{v}_d]}{|\boldsymbol{v}_i|}}{n}. \tag{2}$$

For the n vectors with the cone of internal angle q.

Where $|\boldsymbol{v}_i|$ is the magnitude of vector $\boldsymbol{v}_i$ and k is a scaling constant for the cone angle q.

2.4. Distributions of force directions across the cord

The closeness of force production to an arbitrarily chosen force direction F_b at each point x, y, z in the cord was assessed using the inner product $S_{x,y,z}$ of interpolated direction vector (by normalization of the measured 'active' force, $F_{x,y,z}$ to a unit vector, see above) and the chosen given direction vector F_b.

$$S_{x,y,z} \equiv \langle F_{x,y,z} \cdot F_b \rangle. \tag{3}$$

In this way a three-dimensional map of the scalar $S_{x,y,z}$ which represented the closeness of the force response at a location to a chosen force direction was created. $S_{x,y,z}$ was a variable ranging from -1 representing opposite directions, through 0 representing perpendicular directions, to 1 representing the same direction. These maps were displayed as contour plots or three dimensional isosurfaces on a Silicon Graphics workstation using Explorer software. The scalar map of raw force magnitude regardless of direction was also plotted in this way. Finally, inner product measures at stimulation sites were plotted to validate interpolation procedures.

2.5. Force direction classification

Force directions were classified into groupings using S-plus 3.0 software by the method of *K*-means. The *K*-means technique is a standard statistical method for estimating the numbers and centers of clusters in a data set (Hartigan & Wong, 1979). The Chi square statistic was used to assess quality of classification. We sought to capture 95% of the data variance with our chosen *K*-means centers. The matrix of inner products was also used in nearest neighbour, furthest neighbour and mean distance cluster analyses. Results were similar in all techniques. *K*-means analysis is presented in the results. Forces were also converted to torques using standard algorithms applicable to our recording arrangement (Asada & Slotine, 1986; Kargo & Giszter, 2000a).

2.6. Spatial distributions of forces and their classification

Force patterns across space were examined by generating regular lattices of scalar or vector data using the tesselation and interpolation procedures described in Section 2.2. These data sets could be superimposed graphically for examination.

Correlation of spatial distributions between frogs was examined by calculating the inner-product measure of the samples of one data set and the other data set (Mussa-Ivaldi et al., 1994). The individual standard inner-products of force vectors from the two data sets formed a scalar map of correlation that indicated highly and weakly correlated regions.

It was generally necessary to scale and/or offset individual frog's lumbar cords along the rostro-caudal axis in order to align dorsal root entries. A criterion for choosing the 'best' scaling and offset was required. We used the scaling and offset parameters that generated the highest average sum of individual inner-products (see Mussa-Ivaldi et al. (1994) this measure will be termed "total inner product" in subsequent discussion) while retaining reasonable (>70%) overlap of the cords.

3. Results

3.1. Force production across the cord

Forces and muscle activation patterns were collected in a grid of positions separated by 200 μm mediolaterally and in depth and by 1 mm rostrocau-

dally. Stimulation began at 200 μm below the pia and 200 μm from the midline. Electrode tracks were continued down to 1200 μm depth in 200 μm increments. Stimuli were aligned relative to the caudal junction of the ninth dorsal root entry zone. As we previously (Giszter et al., 1993) observed the active force elicited by the stimulation remained always at the same orientation as it rose to the peak value. Therefore our analyses were concentrated on peak values.

3.1.1. The distribution of forces in the complete sampled populations

We first examined forces across the entire cord as a single population regardless of electrode location. Raw peak forces for one frog are shown in Fig. 2, direction vector distributions are in Fig. 3. It was clear that high magnitude forces clustered in a few directions. We thus also constructed the smoothed force magnitude surfaces. This surface showed how the force magnitude varied as a function of the force direction, for constant current stimulation. The magnitude surfaces for our largest data set spanning the entire lumbar cord are shown in Fig. 4(B). This figure shows the tuning of force magnitude of the population of spinal cord sites stimulated. The population exhibited high magnitude responses in only a few directions, represented as lobes. These lobes represent the presence in the population of a set of sites in which strong forces in specific directions are produced. The smoothed magnitude surface shown in Fig. 4(B) can be 'unfolded' and represented as a surface map using a tangent cylindical projection. This makes the individual tuning peaks easier to visualize. Such a plot is shown in Fig. 5(B) and (D). The tuning of the population's strong force directions could also be demonstrated to be strongly significant using statistical methods. The method of *K*-means was used to examine clustering of directions. This technique clearly demonstrated that a few strong force directions were seen ($p < 0.01$) in the raw peak forces. Each hillock in the magnitude tuning surface of 5(B) represents a peak close to one *k*-mean center.

The *K*-mean directions are summarized in Table 1, and shown as single vectors for the largest data set in Fig. 6(B). In Table 1 we also present the normalized hip and knee joint torques in the horizontal plane that were estimated to be responsible for each *K*-mean end-point force, based on configuration and link lengths. This part of the table shows that two of the force directions represented pure hip extensor and flexor torques. This observation might be predicted based on existing spinal pattern generator results (see Stein & Smith, 1997). However, the other three patterns of joint torque all represented both knee and hip torque associations. One pattern was unique

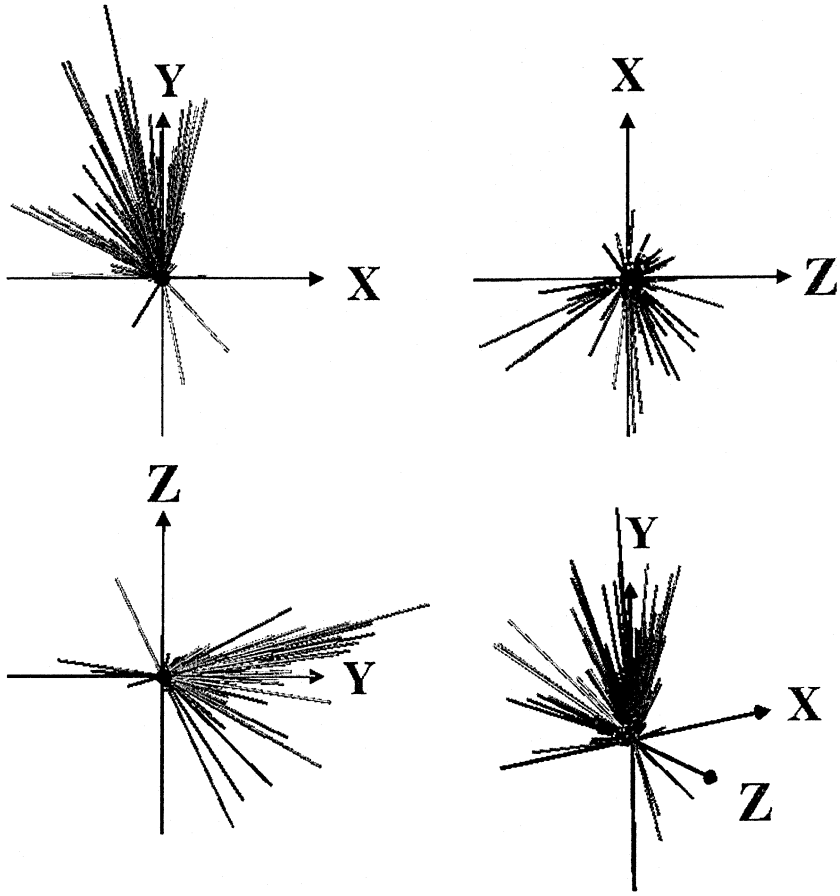

Fig. 2. The population of peak force vectors at 8 μA in a single frog. Both force magnitudes and the force directions produced through the spinal cord in a single frog are represented as a population of vectors in three dimensions. The axes in this figure can be related to body configuration and map data in subsequent figures using Fig. 1(B) and (C) $+X$ is LM, $+Y$ is CR, $+Z$ is DV). Each vector is represented as a variable length cylinder or rod, each of similar diameter, with its base at the origin. Rod length corresponds to magnitude of force, the rod is oriented in the direction of translational force. The population shown derives from our largest data set. Data is shown in perspective in the lower right and is displayed orthographically viewed along the X, Y and Z axes. As previously (Giszter et al., 1993) we observed that the active force elicited remained at the same orientation as it rose to the peak value. Only peak values are shown. It can be seen that in some force directions magnitudes are very large. This implies tuning of the population magnitudes to specific directions. Compare this figure to Fig. 3.

in hip and knee torque balance. The two other patterns were distinguishable from one another using the presence or absence of Z force production indicating an elevator hip torque. This observation reconciles the five

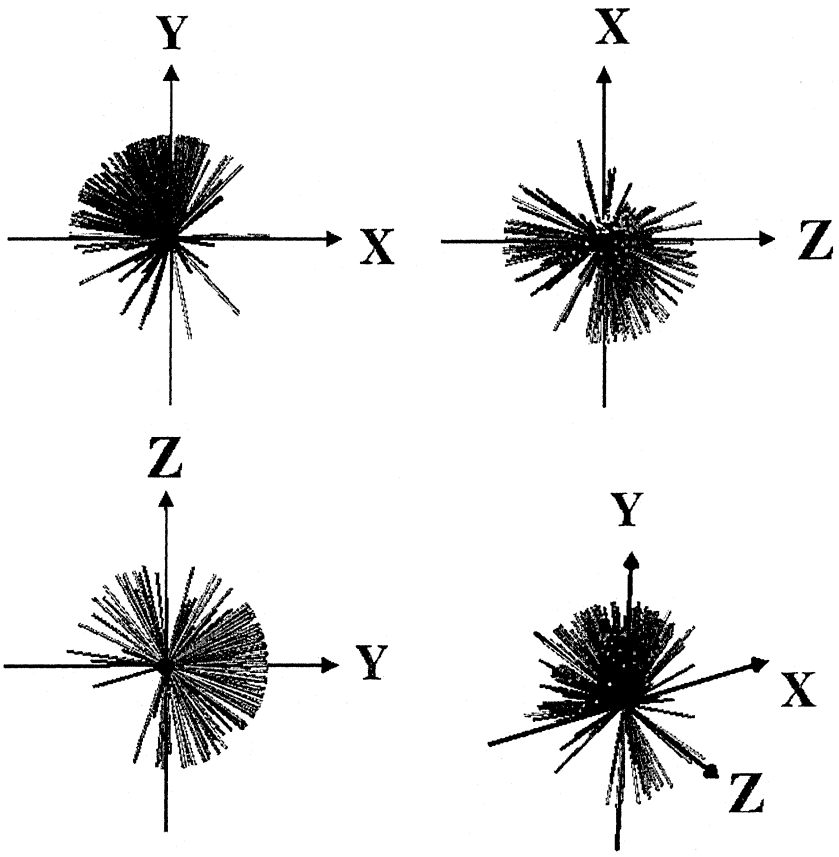

Fig. 3. The population of peak force directions produced in a single frog. The population shown in Fig. 2 has been normalized so that all sites have equal magnitude. The axes in this figure can be related to body configuration and map data in previous and subsequent figures using Fig. 1(B) and (C) ($+X$ is LM, $+Y$ is CR, $+Z$ is DV). Each vector is represented as a constant length cylinder, with its base at the origin. This population derives from our largest data set. Data is shown in perspective in the lower right and displayed orthographically viewed along the X, Y and Z axes. When compared to Fig. 2 it can be seen that the population is more broadly distributed across the sphere of possible directions than suggested by the magnitude plots, indicating large numbers of small forces not evident in Fig. 2. Nonetheless some directions are not represented and others only sparsely represented e.g. in the X/Y plot there are almost no vectors near the X axis and few vectors fall in the bottom right ($+X$, $-Y$) quadrant.

three-dimensional force directions here with the four two-dimensional field types described previously (e.g., Bizzi et al., 1991). There was no pure knee torque pattern in our data. These data therefore support the idea of the production by spinal cord circuitry of pure hip extensor and flexor torque

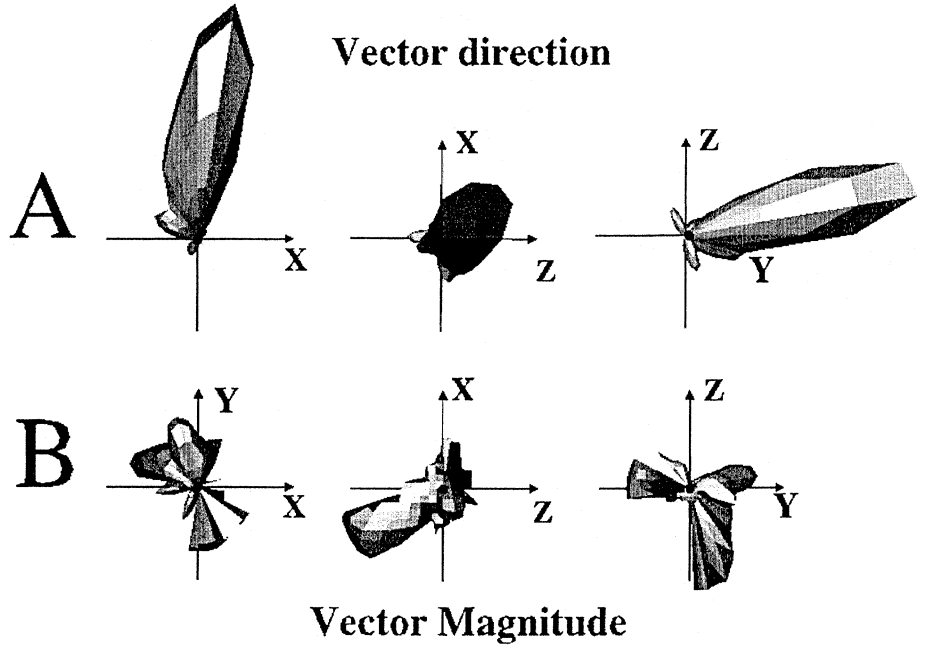

Fig. 4. Smoothed direction density and magnitude tuning of the population responses. The distributions of force probability and force magnitude are shown after the data displayed in Figs. 2 and 3 was smoothed by a simple kernel to generate a continuous surface. The axes in this figure can be related to body configuration and map data in previous and subsequent figures using Fig. 1(B) and (C) ($+X$ is LM, $+Y$ is CR, $+Z$ is DV). (A) Spherical polar plot of the shape of the force probability density in spinal cord. This part of the figure illustrates the force directions most likely to be elicited by a random electrode placement in the spinal cord. The force direction's probability is greatest (has its largest lobe) in a direction that is close to one force magnitude lobe but does not coincide with any of the force magnitude maximum directions. These probability densities were similar among frogs (see Fig. 9). (B) Spherical polar plot of force magnitude tuning in spinal cord. This illustrates the tuning of magnitude to direction for the population. The number of sites representing high magnitude forces may be low compared with the density plot in 4A. Peak force and peaks of probability do not exactly coincide. These surfaces are displayed in tangent cylindrical projections in Fig. 5(A) and (B), where the correspondences and differences are easier to visualize.

patterns, but in addition suggest that coupled multijoint torque patterns are represented in spinal cord, while pure knee torques are absent.

3.1.2. The classification of force directions in the complete sample populations

The strongest forces were only generated in a few directions. These strong forces dominate the magnitude surfaces drawn in Figs. 2, 4(B) and 5(B). However, conceivably other smaller forces could be produced in many other directions throughout the spinal cord. To examine how the smaller forces

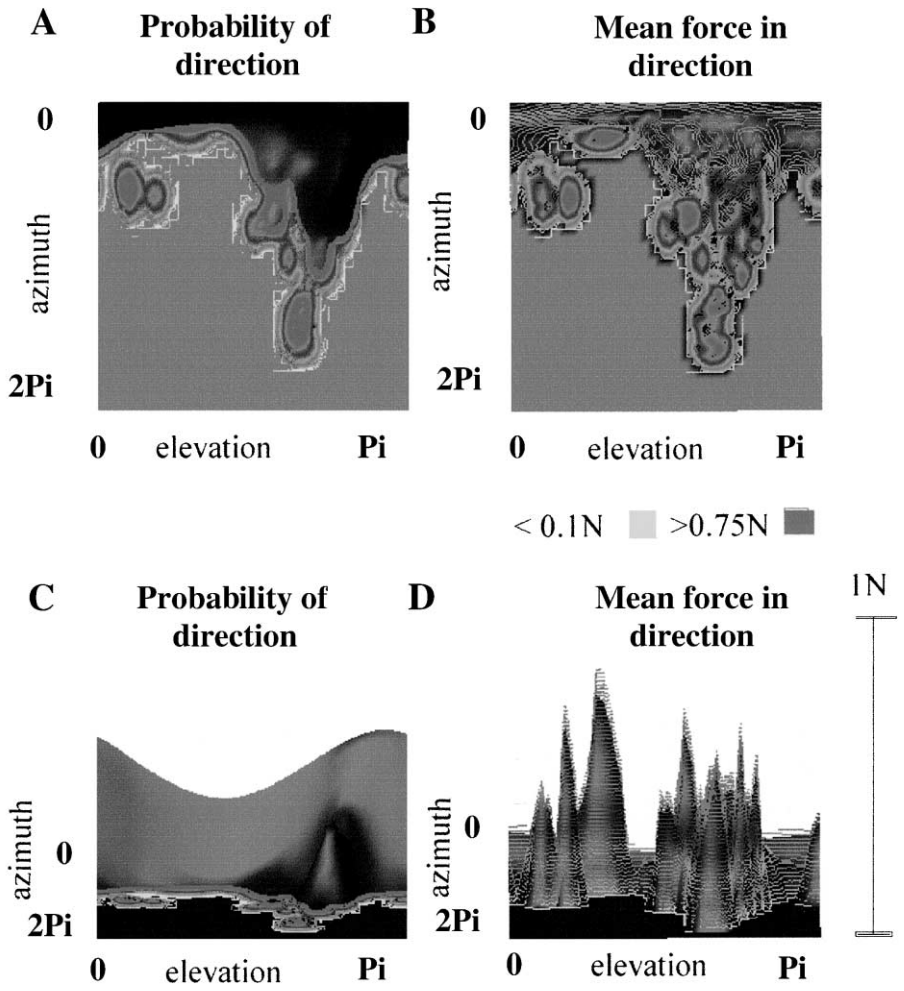

were distributed we normalized the population of forces. By normalizing force vectors at each spinal cord site we obtained distributions of force directions for all sites. These are shown in Fig. 3. It is still clear that only a few directions are strongly represented and some directions not at all. However, we found that a single direction dominated the distribution representing a rostral hip flexion. The method of *K*-means applied to normalized forces also demonstrated that the distribution of directions clustered around a few values ($p < 0.01$). The smoothed normalized force direction vectors provided an estimate of the probability density of directions through spinal cord

Fig. 5. The probability of force direction and the force magnitude expressed as raised surfaces. The polar distributions of Fig. 4 are plotted here in tangent cylindrical projection in which the spherical coordinates of Fig. 4 are projected onto a plane. The axes shown as ordinate (vertical in panels A and B), or away from the viewpoint (in panels C and D) are the azimuth (from 0 to 2Pi) referenced to the mediolateral axis and the abscissas in each (horizontal axes) are the elevation. Elevation runs from 0 to Pi and azimuth from 0 to 2Pi. 0 azimuth is the X axis, 0 elevation is the negative Z axis in the preceding figures. Magnitude of probability or force is expressed as surface height and with contour coloring. Blue contours are low magnitude, green intermediate and red high. In the probability plot the contours do not span the data range. The contours plotted were colour coded and ranges chosen in order to visually emphasize topographic similarities between magnitudes and probabilities distribution. (A) Probability of a force direction in polar coordinates. The surface is viewed orthographically along the Z axis. The largest probability lobe of Fig. 4(A) is now smeared by the projection operation and forms the posterior ridge in this figure. Islands of red contours in this figure have correspondences to the islands of red contours in part B. Note however that these islands represent much lower probability topographic features compared to the large posterior ridge at the figure's top. (B) Average magnitude of a force direction in polar coordinates. The surface is viewed orthographically along the Z axis. Note that the red contours in the foreground each corresponds approximately to the hillocks in the force probability surface in 5(A). (C) Three-dimensional view of the probability surface. (D) Three-dimensional view of the magnitude surface. Scale bar to right indicates 1N. The correspondence of structures shows that each force direction indicated by a magnitude hillock has a significant volume of spinal cord associated with it. The ridge at the back of the plot in 5(C) was uniformly associated with weaker forces in 5(D). Note the large areas (i.e. flat 'planes') of the plots which are unpopulated both in probability and magnitude displays.

Table 1
K-mean centers for magnitude or force direction clustering [a]

	F_X	F_Y	F_Z	τ hip	τ knee
Full vectors					
1	−0.52	0.38	−0.76	0.95	0.32*
2	−0.3	0.93	0.126	1.0	0.09**
3	0.45	−0.88	0.07	−1.0	0.04**
4	−0.89	0.45	0.0	0.92	0.39*
5	0.98	0.0	−0.156	−0.81	0.59
Direction vectors					
1	−0.88	0.44	0.156	0.92	0.39
2	−0.148	0.93	−0.3	0.97	−0.25
3	0.154	0.97	0.156	0.75	−0.66
4	0.0	0.30	−0.95	0.89	−0.44

[a] Normalized force components F_X F_Y and F_Z are tabulated together with calculated horizontal plane joint torques at the knee (τ knee) and about the vertical axis of the hip (or azimuth torques, τ hip). These calculated torques show that pure hip torques form two of the cluster centers in the magnitude data (**). In magnitude based clustering it can also be seen that multi-joint torque patterns 1 and 4 (*) are very similar but can be distinguished based on the component of Z force in the end-point force description. Three of the five magnitude *k*-mean centers and all probability centers represent multi-joint torque patterns. The uniarticular torque patterns in the magnitude centers 2 and 3 appeared to be generally due to balanced coactivation of both uni and multi-articular muscle groups (see e.g. Loeb, Giszter, Saltiel, Mussa-Ivaldi & Bizzi, 1999; Tresch et al., 1999).

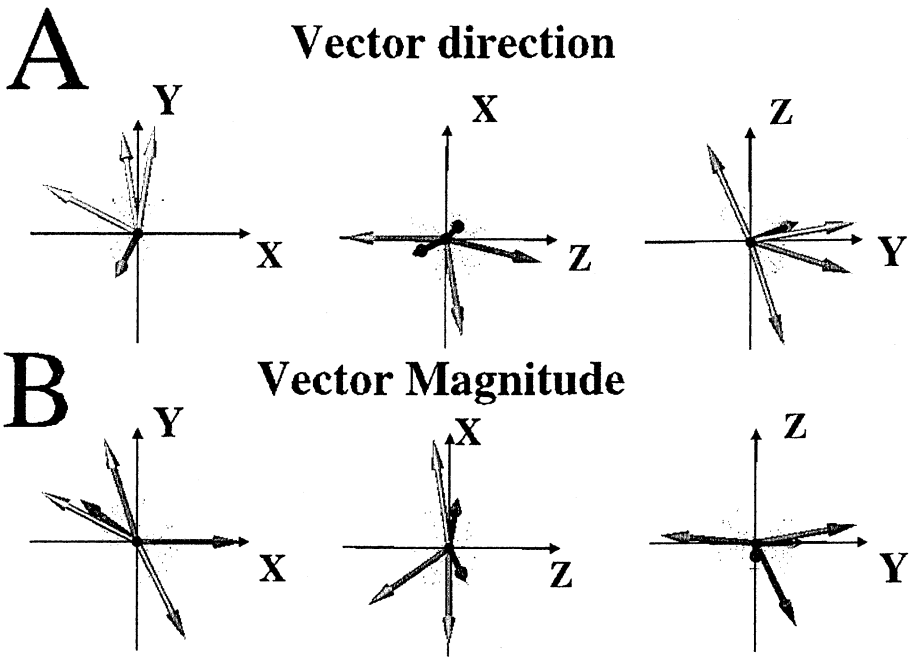

Fig. 6. *K*-means analysis of data in Figs. 2 and 3. The axes in this figure can be related to body configuration and map data in previous and subsequent figures using Fig. 1(B) and (C) ($+X$ is LM, $+Y$ is CR, $+Z$ is DV). (A) *K*-mean cluster directions derived from density of force directions. This figure shows the principle force direction clusters revealed by applying the *K*-means technique to the normalized force directions of the entire spinal cord population. Each vector represents a cluster center. Clusters were significant with $P < 0.01$. Each plot shows the center directions displayed orthographically viewed along the X, Y and Z axes, respectively. Each cluster center represented in this figure corresponds to a lobe in Fig. 3 and a hillock in Fig. 5(A) and (C). (B) *K*-mean cluster directions based on force magnitude. This figure shows the principle force direction clusters revealed by applying the *K*-means technique to the raw peak force vectors of the entire spinal cord population.The three plots show the center directions displayed orthographically viewed along the X, Y and Z axes, respectively. The XY plane plot has directions close to those expected from data in Giszter et al. (1993),Bizzi et al. (1991). Note that in the horizontal plane (XY) components two centers are almost indistinguishable. Note also that the magnitude directions differ from those in the probability density centers shown in A above in some regards. In the earlier work only high magnitude responses were collected.

(Fig. 4(A)). We found that the distributions and *K*-mean directions that were observed in the probability density of population directions differed somewhat from the magnitude based *K*-mean directions. A large lobe of strong hip flexion was found at a direction which was not as prominent in magnitude smoothed plots; this lobe thus represented relatively small elicited forces. This can be seen in Figs. 4(A) and 9(A). The *K*-mean directions for the

normalized force data are summarized in Table 1, and shown as vectors in Fig. 6(A). The peak magnitude clusters were dominated by the high magnitude 'hot spots' of the spinal cord (see Section 3.1.3). In contrast in the density plot there were a larger number of sites in a specific rostral flexion direction where weaker forces were produced as described above. A high magnitude peak lay close to but separate from this peak in the magnitude plot. This is seen more clearly in the projection plots in Fig. 5. The population direction density surfaces of Fig. 4(A) were projected onto a plane to display them in a more conventional way using the tangent cylindrical projection. These surfaces are shown in Fig. 5(A) and (C). Each hillock in the direction density surface of 5(A) represents one *K*-mean center. It can be seen that there is a reasonable correspondence between the 'hills' in the population density (plot 5(A)) and the hills of highest magnitudes (plot 5(B)). Thus in general the directions of high magnitude had high density or probability of occurrence. These patterns were also similar among frogs (see Section 3.1.4). The correspondence means high force directions were also represented in a sizeable volume of spinal cord. However, this population analysis does not address how the volumes in which each direction were elicited were spatially located in spinal cord. The notable exception to the correspondence of magnitude and volume was the particular rostral hip flexion direction that was only represented with lower force magnitudes but accounted for a substantial number of spinal cord sites stimulated. This direction is seen as the large lobe in Fig. 4(A) and the ridge (due to the projection of the 'poles' of a sphere onto a rectangle) in Fig. 5(A). From Table 1 it can be seen that in the torque patterns extracted from the *k*-means of the normalized data (which included the much weaker responses, Fig. 5(A)) all the hip torque flexor patterns were contaminated by knee torques (knee torque >0.1) compared to those in the stronger magnitude based *k*-means patterns which showed more pure hip torques (in Fig. 5(B)).

The population analysis described here clearly demonstrated significant tuning of force production. Only a few force directions were represented in the spinal cord microstimulation data collected by exhaustive mapping. Large ranges of force directions were not observed in the maps in our data sets as can be seen in Fig. 5.

3.1.3. Spatial distribution of force responses

Force classes. Having established that only a few force directions were represented in our data, we next examined the distributions of these force directions across the spinal cord. The regions of high magnitude force were

lower threshold and showed lower force variability. We thus created maps of high magnitude regions from our data. The regions of largest response were mapped using simple thresholding of vector magnitude. Peak magnitudes occurred in the mid lumbar cord around the intermediate layers, and deep or lateral in the grey close to motoneuron pools. Fig. 7 shows these raw forces, and displays the higher magnitude regions as volumes in orthographic views. It can be seen that in addition to forming elongate regions, the magnitude of responses also showed a rostrocaudal periodicity. This periodicity may correspond to the regions identified in the composite maps of Saltiel et al. (1998).

We also mapped the distributions of the main force directions that had been revealed in the population analyses of responses by using the *K*-means technique. We did this without reference to magnitude. This mapping allowed us to examine all sites where the particular force direction occurred in

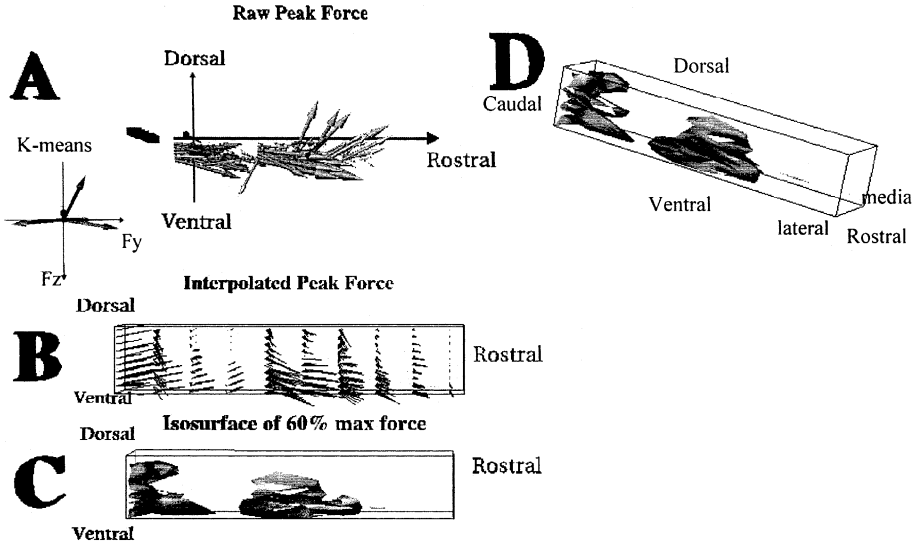

Fig. 7. Regions of high magnitude force responses. The force axes in this figure are as follows (Fig. 1(B) and (C)) *X* is LM, *Y* is CR, *Z* is DV. (A) Raw peak forces (regardless of peak time) expressed as scaled vectors with their base at the stimulation site from which they were elicited. Note grouping of high magnitudes. The *K*-means of raw peak vectors is shown for comparison rotated so that the force coordinate system has positive *Z* down as described in Fig. 1. (B) Interpolated forces at 500 ms after stimulation onset displayed as rods by the Explorer software. Left: lateral view, right: view along the spinal cord rostrocaudal axis. (C) An isosurface extracted from the data using the Explorer software package is displayed. The surface contains the volume of spinal cord of higher force magnitudes (> 0.67 N) regardless of direction of forces. Isosurface at 0.67 N. Left: lateral view, right: view along the spinal cord rostrocaudal axis. (D) Rotated view of the surface in C. Isosurface at 0.67 N.

the spinal cord regardless of the strength of response. To do this we obtained the inner product of normalized sample force vectors with the principal directions of each *K*-mean center at each location in the spinal cord. We then displayed the sites or volumes of tissue in which these inner products were greater than 0.85. The regions thus obtained were elongate three dimensional objects and corresponded to different portions of the grey matter. Different *K*-mean bases directions were represented in different regions. Fig. 8 shows such data for two of the principal directions in a single frog. Besides their elongate features the regions also showed a rostrocaudal periodicity which may correspond to the segmental organization of the lumbar spinal cord's three segments and their dorsal and ventral roots (VII, VIII, IX). However, other directions were represented or recruited in a more fragmentary manner.

3.1.4. Relationships of force spatial distribution among frogs

Force directions and their probability density shapes were very similar among frogs when treated as populations of measurements without regard to spatial location in cord (Fig. 9(A)).

Having established similarity of the limited types of responses from individual frog's lumbar cord, we examined variability of spatial organization of responses between animals. To do this we used an inner product measure to compare force direction maps among frogs. Force patterns at all four current levels in an individual frog were visually similar and locally they correlated well. They were scaled patterns (scaling proportional to current strength, see Giszter et al., 1993). To obtain normative data for correlation we proceeded as follows: We first examined similarity of direction within a single frog at two current strengths (4 and 8 μA). Forces correlated in the same frog at these two different current strengths showed total inner-products (see methods) of 0.8 when the statistic was calculated with the two data sets which were in perfect spatial alignment. We found that this inner product measure rapidly decayed to 0.5 if the cord location of one data set was shifted or scaled along the rostrocaudal axis. This deviation with rostrocaudal movement probably corresponds to the rostrocaudal specialization and (possibly segmental) periodicity remarked on in Section 3.1.3. When comparing among frogs we therefore used data sets from individual frogs that were scaled and offset to obtain their highest total inner-products with other frogs' data. Correlations measured by total inner product techniques among the four most dense and extensive data sets from different frogs ranged from 0.3 to 0.6. The structure and pattern of force distributions in different frogs were thus correlated on the average but much less so than data sets from the same

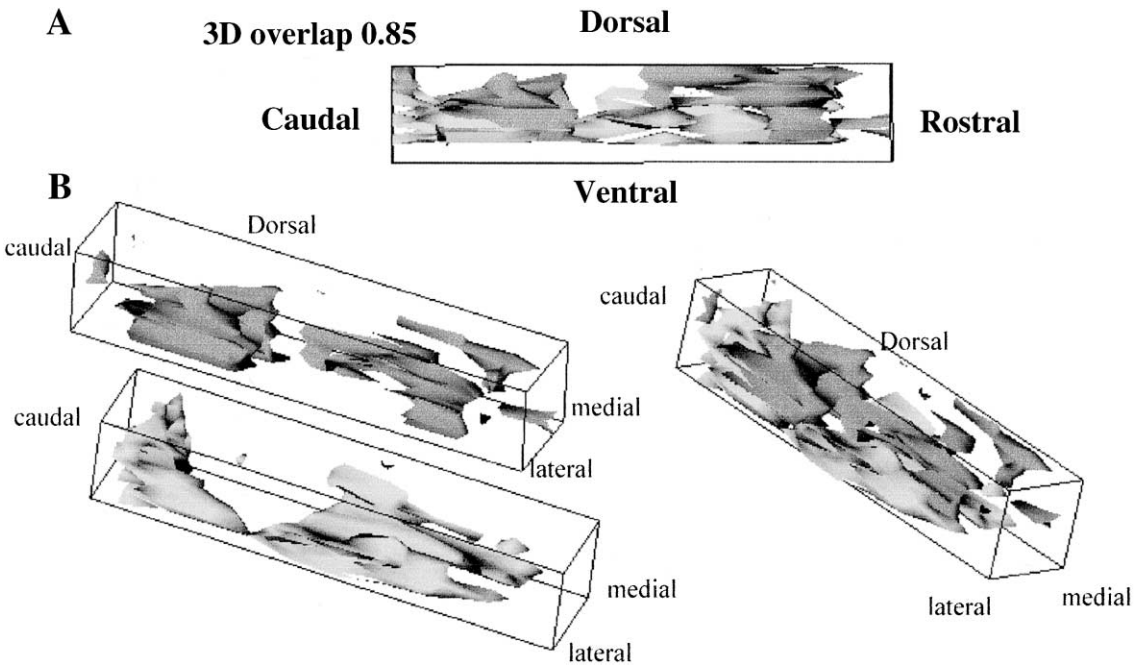

Fig. 8. Regions producing forces close to the first two principle force magnitude directions from Fig. 6(B). (A) The regions of high inner product correlation (>0.85). are displayed as overlapping volumes in lateral view below (basis 1 pink/purple, basis 2 white). The regions of spinal cord in which the force direction vector had an inner product with one or other principle force direction of 0.85 or greater are plotted. Each volume thus comprises forces directed within 25° of the component direction. (B) Below the overlap plot the two volumes are displayed separately in off-axis views. The non overlapping and repeating structure of the two different force directions regions can be seen. Three of the force directions extracted account for most of the volume of grey matter which we stimulated. The remaining directions are more sparsely represented.

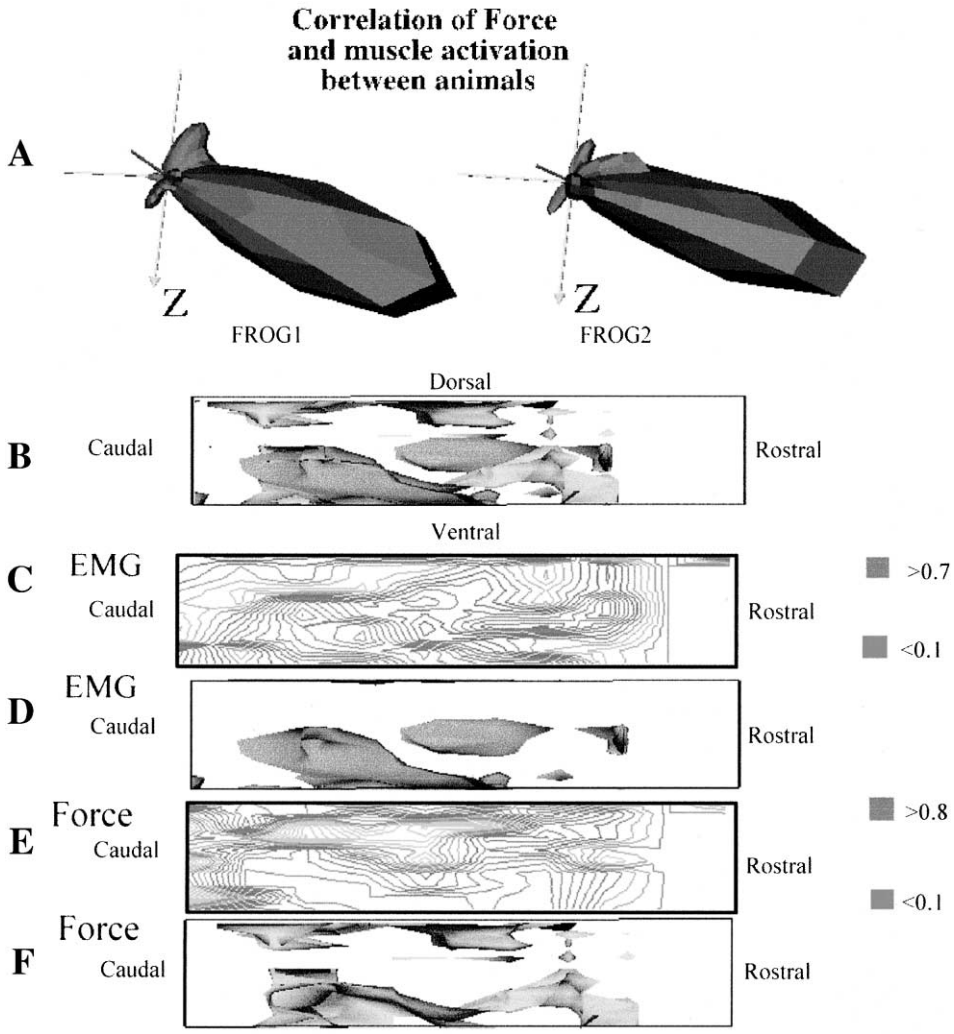

Fig. 9. Similarity among frog spinal cords. (A) shapes of estimated probability densities of peak force directions in two different frogs showing the close similarity of these. (B) Regions of spinal cord in two frogs which correlated strongly. The inner product between force or electromyogram vectors between two frogs were calculated. Regions which had force vectors within 25° of one another (correlation 0.9) and those that had EMG with correlation of 0.7 (angle 45° between 11-dimensional vectors) are plotted. The regions are shown as overlapping volumes. Force regions are pink, EMG white. The volumes are partly overlapping. (C) The correlations of EMG are shown as contours on the parasagittal plane 400 μm from the midline. Red contours are high, blue low. (D) The correlations are shown as volumes of tissue with highly correlated EMG responses in lateral and rostral views. (E) The correlations of peak force are shown as contours on the parasagittal plane 400 μm from the midline. Red contours are high, blue low. (F) The correlations are shown as volumes of correlated tissue in lateral and rostral views (correlation >0.9). This figure shows that regions of consistent correlation between frogs exist for both force and EMG patterns. Note that force patterns correlate in dorsal spinal cord while EMG patterns do not.

frog at two current strengths. Having located the best alignment of two spinal cords we then examined how closely correlated different regions of spinal cord were. We used the local inner product of normalized force or EMG as a measure to map spinal cord regions of high correlation. We found that specific regions of spinal cord correlated very strongly (inner product measures >0.9). The regions of high correlation could be detected as high inner-products between normalized sample forces in each frog. Fig. 9(B) shows a region of high correlation between forces in two frogs as surfaces and as contours in the 400 μm parasagittal plane. This figure also shows regions of EMG correlation. Relations of EMG data to forces will be presented and analyzed in more detail in a later paper. Although not exactly overlapping, these regions were in similar locations. EMG correlation was less strong. We were using an inner product measure of correlation for all the eleven recorded muscles. The lower correlation is in keeping with the likelihood of inter-animal variation of electromyogram pickup, which would diminish correlation, and the higher dimension of the EMG data (and see Loeb, 1995; Loeb et al., 1999). Finally, Fig. 9 also shows a composite overlap of the volumes of spinal cord that correlate strongly. It can be seen that the dorsal horn, ventral horn and lower intermediate zones have substantial regions of correlations. Forces correlate among frogs more strongly than EMGs in the upper dorsal horn.

4. Discussion

Mapping in any domain is fraught with difficulty (see for example Monmonier, 1991). Previous studies of cord topography have used various methods. For example they have mapped the receptive fields of afferents (Joseph & Whitlock, 1968; Brown, 1981), mapped field potentials and interneuron groups associated with behaviors (Noga et al., 1995), mapped activity related markers associated with behaviors (Barajon, Gossard & Hultborn, 1992; Kjaerulff, Barajon & Kiehn, 1994), mapped distributions of neurotransmitter receptors, cell types in different regions and motor nuclei (e.g. Cruce, 1974). Microstimulation as a mapping technique has been used in various brain structures (e.g. Donoghue & Wise, 1982; Drew & Rosingnol, 1990; Robinson & Fuchs, 1969). In spinal cord it has been used primarily to identify connectivity (Gustafsson & Jankowska, 1976), or to identify ventral horn motor responses and motor pool locations for design of functional electrical stimulation (FES) therapies (Mushahwar & Horch, 1997;

Mushahwar, 1996; Tai, Booth, Robinson, DeGroat & Roppolo, 1997; Grill & Wang, 1997; Grill & Bhadra, 1996; Giszter et al., 2000; Lemay and Grill, 2000).

In choosing the density of mapping data collection and the methods of analysis one must compromise between resolution and feasibility. The data collected here extend the microstimulation described previously, to include responses throughout the grey matter of the frog lumbar spinal cord. Most previous stimulation in frogs was concentrated around 6–800 μm in depth. This study expanded the volume of cord examined to include the dorsal and ventral horns in the lumbar regions. To do this it was necessary to reduce the number of configurations of limb examined. The currents we used here were small and the activity elicited is likely to often represent predominantly the activity of cells (Saltiel & Bizzi, 1994; Saltiel et al., 1998). Microstimulation at 8 μA (our largest current) was expected to activate a sphere of cells within 100 μm of the electrode tip, probably only a few hundred to a thousand neurons (see Yeomans, 1990). The description here of regions of similar force production thus are most likely to have arisen from stimulation of spatially separate clusters of cells at each site. The cells at such sites may represent either similar spinal cord organization at the similar sites, or else different types of sites ultimately funnelling their activity to circuits of similar motor actions or functional end-points.

The types of forces obtained here fell into a few clusters regardless of site in spinal cord stimulated. This study was thus in keeping with previous work with smaller data sets. Further, our data allowed the lower threshold and larger force magnitude sites of each cluster to be localized within areas of spinal cord. This demonstration of localization may have relevance for future applications of intraspinal functional electrical stimulation (see Mushahwar & Horch, 1997). We found that the structure of the strong force producing regions appeared to have a rostrocaudally repeating structure. This structure was obscured in the earlier studies by pragmatic limitations on extent of stimulation. This study did not suffer from that limitation but instead suffered the limitation of examining only a single limb configuration. It is conceivable that variations of force production could occur at other limb configurations which would go unnoticed in this study. The presence of pure hip flexor and extensor torques as clusters in the data set is in keeping with several descriptions of spinal cord organization (see Stein & Smith, 1997). In particular, the pure hip torque patterns can be closely associated with a bilaterally distributed pattern generation system in turtle spinal cord. The additional presence of multi-joint torque patterns and the absence of any pure knee

torques in our data may also be significant. The data support the suggestion that frog spinal cord may specifically organize hip torques and controls of uniarticular hip muscles, but also organizes the control of specific proximal multi-joint limb biomechanics patterns by using biarticular muscles in multi-joint groupings. The importance of multi-joint coupling and biarticular muscles has been emphasized in several contexts (see Hogan, 1985; Gielen, 1993; Nichols, 1994). Organization of such coupled multi-joint torque patterns in spinal cord may be required for precise reflex and pattern generator limb control throughout the significant workspace covered by frog hindlimbs.

In this study, we explored in some detail the pattern of responses in the dorsal and ventral horns. Stimulation of both the superficial cutaneous regions and deeper proprioceptive and intermediate regions gave patterned force responses that matched with previous experimental data. However correlation of EMG patterns among frogs was substantially better in intermediate zone and ventral horn (Section 3.1.4 and Fig. 9). In the ventral horn broad but rostrocaudally localized muscle activity occurred. However, in this set of experiments we did not observe focal activations of single muscle pools.

Because of the extensive dendritic arbors of motoneurons in frogs the possibility of direct activation of motor pools is a concern in microstimulation in frog spinal cord. We have controlled this and addressed this previously in several ways (Giszter et al., 1993). The current data set also helps address these concerns. Some parts of the cord showed little response in dense mapping. The arborization patterns of motoneuron dendrites and the topography of motoneuron density (Cruce, 1974; Bregman & Cruce, 1985; Rosenthal & Cruce, 1985) would not explain these differences.

In comparing frogs we observed a good correlation of force and EMG pattern between some regions of spinal cord. This suggested that a common topography and structure underlay much of the spinal cord organization, confirming aspects of our earlier studies. However EMG also differed from animal to animal somewhat. It is plausible that differences among individual frogs may result from motor-equivalent developmental variations. However, some of the variability could also be attributed to other factors such as variations in muscle electrode placement, spurious activation of motoneurons in different animals, or variations in threshold and post transection spinal cord state from animal to animal. Given these different potential sources of variability, the similarity of some aspects of cord response topography is probably the most salient finding in comparing among frogs. This finding suggests that intraspinal electrodes might be placed in topographically

defined spinal cord interneuronal systems for multi-joint controls in functional electrical stimulation applications (see Mushahwar & Horch, 1997, 2000; Mushahwar, 1996; Tai et al., 1997; Grill & Wang, 1997; Lemay & Grill, 1999; Giszter et al., 2000).

Giszter et al., 1993 showed the similarity of force-fields and motor responses elicited by natural skin stimulation and force-fields and motor responses elicited by microstimulation of spinal cord. The similarity of such responses suggests the organization of the deeper motor responses elicited may relate to the sensory topography of the overlying spinal cord. In rats this relationship is well understood (Tresch, 1997; Schouenberg, 1984; Tresch & Bizzi, 1999). Work of Tresch et al. (1999) suggests that at upper levels of spinal cord a sensory map responsible for recruiting combinations of muscles or synergies is present in frog spinal cord. Contralateral responses are also recruited by microstimulation and these are discussed in detail in the context of functional electrical stimulation applications in Giszter et al. (2000).

In conclusion, this data set provides a map to spinal cord regions where microstimulation is particularly effective. Specific regions generate multi-joint hip/knee torque patterns or pure hip torques, but never pure knee torques. These regions have a specific topography which shows some rostrocaudal repetition. These regions are suitable targets for recording or pharmacological activation, or tracing techniques. Further, the data support the notion of a few types of force response patterns that can be elicited by microstimulation. In the future it may be possible to associate these with specific groups of interneurons, active in sensorimotor integration or pattern generation, a few patterns of EMG or drives to motor pools in a given animal. Although forces fall into a small set, it is possible that the underlying motor activity is more complex even in its simplest and lowest dimensional representations, and any given force pattern may be generated by differing muscle activations. Taken in total, the results are in keeping with the idea of a set of force-field organizing primitives which are allied to spinal reflexes and spatially ordered in the spinal cord of the frog. Similar results in both rat (Tresch & Bizzi, 1999) and cat (reviewed in Giszter et al., 2000) speak of the possible importance of this approach in an understanding of the development of human coordination strategies (see Gottlieb, 1998; Zaal et al., 1999). Spinal circuitry in humans may retain much of the modularity and structure observed in lower tetrapods and other mammals (Bussel, Roby-Brami, Neris & Yakovleff, 1996; Calancie, Needham-Shropshire & Jacobs, 1994; Edgerton et al., 1992; Harkema et al., 1997). Quantization of movement and low dimensional groupings have also been observed in man (Gribble, Ostry, Sanguineti &

Laboissiere, 1998; Krebs, Aisen, Volpe & Hogan, 1999; Pigeon, Yahia, Mitnitski & Feldman, 2000; Raasch & Zajac, 1999). Plainly rehabilitation of human motor control after injury using traditional approaches (Harkema et al., 1997) and neuroprosthetic approaches using cortical (Chapin, Moxon, Marlowitz & Nicolelis, 1999) or spinal circuitry (Giszter et al., 2000) will benefit from an understanding of these mechanisms and their comparative organization across species and through development.

Acknowledgements

Supported by NIH NS09343 and ONR N00014-95-I-0445 to EB, and NS34640 and an ASRI equipment grant to SFG. Drs. M. Pinter and P Saltiel, M Tresch and JS Schotland offered helpful discussions at various stages of the analysis. Anonymous reviewers provided extensive comments which have improved presentation and clarity. The authors would also like to acknowledge the Santa Fe Institute's support of the conference "Debates in Dynamics" at which this data and related topics were discussed and which was organized by Dr. Dagmar Sternad, a Santa Fe Institute Fellow-at-Large.

References

Asada, H. & Slotine, J. J. E. (1986). *Robot analysis and control*. Wiley: New York.

Barajon, I., Gossard, J. P. & Hultborn, H. (1992). Induction of fos expression by activity in the spinal rhythm generator for scratching. *Brain Research*, *588* (1), 168–172.

Bernstein, N. (1967). *The coordination and regulation of movements*. Pergamon Press: New York.

Bizzi, E., Mussa-Ivaldi, F. A. & Giszter, S. F. (1991). Computations underlying the execution of movement: A novel biological perspective. *Science*, *253*, 287–291.

Bregman, B. S. & Cruce, W. L. R. (1985). Normal dendritic morphology of frog spinal motoneurons: A golgi study. *Journal of Computer Neurology*, *193*, 1035–1045.

Bussel, B., Roby-Brami, A., Neris, O. R. & Yakovleff, A. (1996). Evidence for a spinal stepping generator in man. Electrophysiological study. *Acta Neurobiologiae Experimentalis*, *56* (1), 465–468.

Calancie, B., Needham-Shropshire, B. & Jacobs, P. et al. (1994). Involuntary stepping after chronic spinal cord injury. Evidence for a central rhythm generator for locomotion in man. *Brain*, *117*, 1143–1159.

Cannon, M. & Slotine, J. J. E. (1995). Space frequency localized basis networks for nonlinear estimation and control. *Neurocomputing*, *9* (3).

Chapin, J. K., Moxon, K. A., Marlowitz, R. S. & Nicolelis, M. A. L. (1999). Realtime control of a robot arm usingsimultaneously recorded neurons in the motor cortex. *Nature Neuroscience*, *2* (7), 664–670.

Cruce, W. L. R. (1974). The anatomical organization of hind-limb motoneurons in the lumbar spinal cord of the frog, Rana catesbiana. *Journal of Computer Neurology*, *153*, 59–76.

Donoghue, J. P. & Wise, S. P. (1982). Rat motor cortex: Cytoarchitecture and microstimulation mapping. *Journal of Computer Neurology*, *212*, 76–88.

Drew, T. & Rossignol, S. (1990). Functional organization of the medullary reticular formation of intact unanaesthetized cat II: Electromyographic activity evoked by microstimulation. *Journal of Neurophysiology*, *64*, 782–795.

Edgerton, V. R., Roy, R. R., Hodgson, J. A., Prober, R. J., De Guzman, C. P. & de Leon, R. (1992). Potential of adult mammalian lumbosacral spinal cord to execute and acquire improved locomotion in the absence of supraspinal input. *Journal of Neurotrauma*, *9*, 110–127.

Gandolfo, F., Mussa-Ivaldi, F. A. & Bizzi, E. (1996). Motor learning by field approximation. *Proceedings of the National Academy of Sciences of the United States of America*, *93* (9), 3843–3846.

Giszter, S. F. & Kargo, W. J. (2000). Conserved temporal dynamics and vector superposition of primitives in frog wiping reflexes during spontaneous extensor deletions. *Neurocomputing*, *32/33*, 775–783.

Giszter, S. F., Grill, W., Lemay, M., Mushahwar, V. & Prochazka, A. (2000). Intraspinal microstimulation, techniques, perspectives and prospects for FES. In J. K. Chapin, K. A. Moxon (Eds.), *Neural prostheses for restoration of sensory and motor function*. Boca Raton, FL: CRC Press.

Giszter, S. F., Mussa-Ivaldi, F. A. & Bizzi, E. (1993). Convergent force fields organized in the frog spinal cord. *Journal of Neuroscience*, *13*, 467–491.

Gielen, S. (1993). Muscle activation patterns and joint angle coordination in multijoint movements. In C. Gielen, V. Henn, K. P. Hoffmann, M. Imbert, F. Lacquaniti, A. Rocoux, P. Viviani & J. Van Gisbergen (Eds.), *Multisensory control of movement* (pp. 293–313). Oxford.

Gottlieb, G. L. (1998). Muscle activation patterns during two types of voluntary single-joint movement. *Journal of Neurophysiology*, *80* (4), 1860–1867.

Gribble, P. L., Ostry, D. J., Sanguineti, V. & Laboissiere, R. (1998). Are complex control signals required for human arm movement? *Journal of Neurophysiology*, *79* (3), 1409–1424.

Grill, W. M. & Wang, B. (1997). Mapping knee torques evoked by intraspinal microstimulation. In *Proceedings of the 19th annual international conference*, IEEEEMBS.

Grill, W. M. & Bhadra, N. (1996). Genitourinary responses to microstimulation of the sacral spinal cord. *Society for Neuroscience Abstracts*, *22*, 1842.

Gustafsson, B. & Jankowska, E. (1976). Direct and indirect activation of nerve cells by electrical pulses applied extracellularly. *Journal of Physiology*, *258*, 33–61.

Harkema, S. J., Hurley, S. L., Patel, U. K., Requejo, P. S., Dobkin, B. H. & Edgerton, V. R. (1997). Human lumbosacral spinal cord interprets loading during stepping. *Journal of Neurophysiology*, *77*, 797–811.

Hartigan, J. A. & Wong, M. A. (1979). A *k*-means clustering algorithm. *Applied Statistics*, *28*, 100–108.

Hogan, N. (1985). The mechanics of multi-joint posture and movement control. *Biological Cybernetics*, *52*, 315–331.

Joseph, B. S. & Whitlock, D. G. (1968). Central projections of selected spinal dorsal roots in anuran amphibians. *Anatomical Record*, *160*, 279–288.

Kargo, W. J. & Giszter, S. F. (2000a). Rapid correction of aimed movements by summation of force-field primitives. *Journal of Neuroscience*, *20* (1), 409–426.

Kargo, W. J. & Giszter, S. F. (2000b). Afferent roles in hind-limb wiping reflex trajectories: Free limb kinematics. *Journal of Neurophysiology*, *43*, 1480–1501.

Kiehn, O., Hounsgard, J. & Sillar, K. T. (1997). Basic building blocks of vertebrate cpgs. In P. S. G. Stein, S. Grillner, A. I. Selverston & D. G. Stuart (Eds.), *Neurons networks and motor behavior* (pp. 47–60). Cambridge MA: MIT press.

Kjaerulff, O., Barajon, I. & Kiehn, O. (1994). Sulphorhodamine-labelled cells in the neonatal rat. *Journal of Physiology*, *478* (Pt2), 265–273.

Krebs, H. I., Aisen, M. L., Volpe, B. T. & Hogan, N. (1999). Quantization of continuous arm movements in humans with brain injury. *PNAS*, *96* (8), 4645–4649.

Lemay, M. A. & Grill, W. M. (1999). Endpoint forces evoked by microstimulation of the cat spinal cord, presented at 21th Annual International Conference of the IEEE/EMBS and Annual Fall Meeting of the BMES, Atlanta, GA.

Loeb, E., Giszter, S. F., Borghesani, P. & Bizzi, E. (1993). Effects of dorsal root cut on forces evoked by spinal microstimulation in the spinalized frog. *Journal of Somatosensory and Motor Research*, *10* (1), 81–95.

Loeb, E. P., Giszter, S. F., Saltiel, P., Mussa-Ivaldi, F. A. & Bizzi, E. (1999). Output units of motor behavior: An experimental and modeling study. *Journal of Cognitive Neuroscience*, *12*, 1–20.

Loeb, G. E. (2000). Overcomplete musculature or underspecified tasks? *Motor Control 4* (1), 81–83; discussion 97–116.

Lohmiller, W. & Slotine, J. J. (1998). On contraction analysis for nonlinear systems. *Automatica*, *34*, 683–696.

Lorenson, W. E. & Cline, H. E. (1987). Marching cubes: a high resolution 3D surface reconstruction algorithm. *Computer Graphics*, *21* (3), 163–169.

Mataric, M. J., Williamson, M. M., Demiris, J. & Molan, A. (1998). Behavior-based primitives for articulated control. *Proceedings of the SAB 98*, Zurich, Switzerland.

Monmonier, M. (1991). *How to lie with maps*. Chicago: University of Chicago Press.

Mushahwar, V. K. (1996). *Feasibility of spinal cord stimulation for control of lower extremities in paraplegia*. Ph.D. Thesis, University of Utah, Salt Lake City, UT.

Mushahwar, V. K. & Horch, K. W. (1997). Proposed specifications for a lumbar spinal cord electrode array for control of lower extremities in paraplegia. *IEEE Transactions on Rehabilitation Engineering*, *5*, 237–243.

Mushahwar, V. K. & Horch, K. W. (2000). Selective activation of muscles in the feline hind-limb through electrical microstimulation of the ventral lumbo-sacral spinal cord. *IEEE Transactions on Rehabilitation Engineering*, in press.

Mussa-Ivaldi, F. A. (1992). From basis functions to basis fields: Using vector primitives to capture vector patterns. *Biological Cybernetics*, *67*, 479–489.

Mussa-Ivaldi, F. A. & Gandolfo, F. (1993). Vector summation of endpoint impedance in kinematically redundant manipulators. *Conference on Intelligent Robots and Systems*, *3*, 1627–1634.

Mussa-Ivaldi, F. A. & Giszter, S. F. (1992). Vector field approximation: A computational paradigm for motor control and learning. *Biological Cybernetics*, *67*, 491–500.

Mussa-Ivaldi, F. A. (1997). Nonlinear force fields: A distributed system of control primitives for representing and learning movements. In *Proceedings of the IEEE international symposium on computational intelligence in robotics and automation*. Monterey, CA.

Mussa-Ivaldi, F. A. Giszter, S. F. & Bizzi, E. (1994). Linear superposition of primitives in motor control. *Proceedings and National Academy of Sciences*, *91*, 7534–7538.

Nichols, T. R. (1994). A biomechanical perspective on spinal mechanisms of coordinated muscular action: An architecture principle. *Acta Anatomica*, *151* (1), 1–13.

Noga, B. R., Fortier, P. A., Kriellaars, D. J., Dai, X., Detillieux, G. R. & Jordan, L. M. (1995). Field potential mapping of neurons in the lumbar spinal cord activated following stimulation of the mesencephalic locomotor region. *Journal of Neuroscience*, *15*, 2203–2217.

Pigeon, P., Yahia, L. H., Mitnitski, A. B. & Feldman, A. G. (2000). Superposition of independent units of coordination during pointing movements involving the trunk with and without visual feedback. *Experimental Brain Research*, *131* (3), 336–349.

Preparata, F. P. & Shamos, M. I. (1988). *Computational geometry*. New York: Addison-Wesley.

Raasch, C. C. & Zajac, F. E. (1999). Locomotor strategy for pedaling: Muscle groups and biomechanical functions. *Journal of Neurophysiology*, *82*, 515–525.

Robinson, D. A. & Fuchs, A. F. (1969). Eye movements evoked by stimulation of the frontal eye fields. *Journal of Neurophysiology*, *32*, 637–648.

Rosenthal, B. M. & Cruce, W. L. R. (1985). The dendritic extent of motoneurons in frog brachial spinal cord: A computer reconstruction of HRP filled cells. *Brain Behavioural Evolution*, *27*, 106–114.

Saltiel, P. & Bizzi, E. (1994). Focal intraspinal NMDA iontophoresis produces distinct activation patterns in the frog. *Society for Neuroscience Abstracts*, *20*, 1406.

Saltiel, P., Tresch, M. & Bizzi, E. (1998). Spinal cord modular organization and rhythm generation: An NMDA iontophoretic study in the frog. *Neurophysiology*, *80*, 2323–2339.

Schouenborg, J. (1984). Functional and topographical properties of field potentials evoked in rat dorsal horn by cutaneous C fiber stimulation. *Journal of Physiology*, *356*, 169–192.

Stein, P. S. G. & Smith, J. L. (1997). Neural and biomechanical control strategies for different forms of vertebrate hind-limb motor tasks. In P. S. G. Stein, S. Grillner, A. I. Selverston, D. G. Stuart (Eds.), *Neurons networks and motor behavior*. Cambridge, MA: MIT Press.

Tai, C., Booth, A. M., Robinson, C. J., DeGroat, W. C. & Roppolo, J. R. (1997) Mapping of sites in the cat lumbar spinal cord which produce hind-limb flexion and extension to focal microstimulation. *Society for Neuroscience Abstracts*, *299* (1).

Tresch, M. (1997). *Discreteness of the spinal motor systems in rat and frog*. Ph.D. thesis. Cambridge, MA: MIT Press.

Tresch, M., Saltiel, P. & Bizzi, E. (1999). The construction of movement by the spinal cord. *Nature Neuroscience*, *2*, 162–167.

Tresch, M. C. & Bizzi, E. (1999). Responses to spinal microstimulation in the chronically spinalized rat and their relationship to spinal systems activated by low threshold cutaneous stimulation. *Experimental Brain Research*, *129*, 401–416.

Windhorst, U. R. (1991). Group report What are the units of motor behavior and how are they controlled? In D. R. Humphrey, H. J. Freund (Eds.), *Motor control: Concepts and issues* (pp. 101–120). Wiley: New York.

Yeomans, J. S. (1990). *Principles of brain stimulation*. Oxford: Oxford University Press.

Zaal, F. T., Daigle, K., Gottlieb, G. L. & Thelen, E. (1999). An unlearned principle for controlling natural movements. *Journal of Neurophysiology*, *82* (1), 255–259.